Sustainable Structures
ISSN: 2789-3111 (Print); ISSN: 2789-312X (Online)
http://www.sustain-dpl.com/journal/sust
DOI: 10.54113/j.sust.2026.000106

ORIGINAL ARTICLE

Assessing environmental impact through Computational Structural Optimization

Laura Sardone [a*], Giulia Angelucci [b]

[a] Politecnico di Torino, Department of Structural, Geotechnical and Building Engineering, 10129 Torino, Italy
[b] Sapienza University of Rome, Department of Structural and Geotechnical Engineering, 00184 Rome, Italy
[*]Corresponding Author: Laura Sardone. Email: laura.sardone@polito.it

Abstract: The urgent need to reduce the construction sector's environmental footprint is prompting a shift towards more sustainable methodologies. Traditional construction practices, marked by excessive resource consumption and high emissions, require immediate transformation. With their stringent energy and emission targets, European policies emphasize the critical role of integrated Life Cycle Assessment (LCA) in accurately evaluating sustainability. In this context, Structural Optimization (SO) techniques represent a powerful tool for incorporating environmental metrics within holistic design paradigms. This study presents a robust framework that synergistically integrates SO techniques with LCA methodologies to estimate and mitigate the environmental impacts of a space-frame structural system. Employing generative computational design techniques, this work leverages the Visual Programming Language (VPL) to define optimal configurations for parametric structural models. Specifically, the optimization process prioritizes material efficiency and Global Warming Potential (GWP) as key environmental metrics by simultaneously optimizing size, shape and topology. The implementation of a Multi-Objective Evolutionary Algorithm (MOEA) yields multiple solutions with the identification of a Pareto-optimal front, balancing structural performance with environmental considerations. This study demonstrates that the adoption of hybrid-material solutions incorporating timber elements can substantially reduce the associated GWP compared to traditional steel systems without penalizing structural efficiency. The results emphasize the importance of integrating environmental parameters within the conceptual design phase to promote sustainability in practical applications within the Architecture, Engineering and Construction (AEC) field.

Keywords: Life Cycle Assessment, Structural Optimization, Environmental Engineering, Steel Structures, Sustainable Construction

1 Introduction

The growing recognition of the construction sector's major role in global carbon emissions and resource depletion has driven a shift towards more sustainable building practices. Traditional construction practices, indeed, are characterized by material overconsumption and substantial environmental impact. Evidence from recent studies demonstrates that the Architecture, Engineering, and Construction (AEC) industry is a primary driver of global Carbon Dioxide (CO_2) emissions and is responsible for approximately 40% of total greenhouse gas (GHG) emissions and energy consumption

Received: 11 March 2024; Received in revised form: 4 February 2026; Accepted: 8 May 2026

worldwide [1]. Within the European Union, building construction alone is responsible for 36% of CO_2 emissions and 40% of energy consumption [2]. Acknowledging these environmental imperatives, and in alignment with European policy initiatives such as the Energy Performance of Buildings Directive (EPBD) [3] and the European Green Deal [4], contemporary structural engineering is actively directed towards the development of more sustainable and efficient structures. Indeed, these directives establish stringent targets for energy efficiency and carbon emission reduction in the built environment, driving innovation in material selection, construction technologies, and maintenance [5]. Achieving sustainability requires a more strategic allocation of structural materials, offering both environmental and economic benefits.

In this context, a comprehensive Life Cycle Assessment (LCA), which evaluates the environmental impact of a product or system throughout its complete life cycle (from raw material extraction to end-of-life disposal) as regulated by ISO 14044:2006 [6] and 14040:2006 [7], is paramount for the rigorous quantification of construction material sustainability. While global efforts aim to reduce energy consumption and GHG emissions, the research community also places significant emphasis on enhancing structural performance efficiency of buildings [8]. The identification of solutions that satisfy multiple, often conflicting, objectives within the design process — including cost reduction, structural performance improvement, material minimization, and CO_2 emission abatement — renders the implementation of automated optimization techniques essential for navigating complex design spaces.

Structural Optimization (SO) is a multidisciplinary approach that combines engineering principles with computational tools to improve structural efficiency. In the AEC industry, optimization methods are typically divided into size, shape, and Topology Optimization (TO). Size optimization focuses on determining optimal Cross-Sections (CSs) of structural members [9],[10], shape optimization aims to find the best geometric configuration of structural boundaries [1], [11], while TO addresses the optimal material distribution within a predefined design domain [12], [13]. However, such classification is purely theoretical since these methods are often combined within hybrid frameworks [14], which provide substantially improved structural efficiency and a powerful tool for achieving high-performance and lightweight designs [15], [16]. A key limitation of traditional SO techniques is their focus on structural objectives, such as maximizing performance indicators (e.g., stiffness, strength, energy dissipation capacity) and minimizing material use, often neglecting environmental impact. Nonetheless, the integration of these multifaceted factors within a holistic framework is indispensable for the development of successful, performant designs. Such an approach, in fact, enables a quantitative assessment of the trade-offs between disparate design parameters, fostering informed decision-making that reconciles structural performance, economic viability, and environmental responsibility. Consequently, SO techniques have evolved to address these limitations [17], [18]. This evolution has prompted the incorporation of LCA as a critical decision-making criterion within optimization frameworks [19].

Within SO, LCA has been applied to several structural types to assess and enhance environmental performance. In automotive design, for instance, LCA is employed for Body-In-White (BIW) structures considering different variables, such as material selection, vehicle life, and recyclability [20]. Similarly, in building design, LCA-BIM integration facilitates the comparative analysis of different structural systems, assisting designers to prioritize actions that mitigate environmental impact [21]. Integrated design approaches employing Multi-Objective Optimization (MOO) techniques have recently emerged for integrating LCA with SO. These computational approaches permit the direct integration of environmental impact metrics into the design workflow, ensuring that sustainability considerations are embedded from the initial stages of design. For instance, the Eco-OptiCAD methodology combines SO and LCA tools to support designers in improving product environmental performance while maintaining structural and functional requirements [22]. This approach uses virtual prototyping tools, function modelling, and LCA to generate alternative green scenarios based on shape, material, and production parameters. The strategy empowers designers to achieve more efficient solutions by prioritizing environmental objectives alongside traditional structural and cost requirements.

As this field continues to advance, the development of more sophisticated tools and methodologies to streamline the definition of sustainable structures is anticipated [23], [24]. For instance, Drewniok et al. (2020) developed the Lightest Beam Method (LBM) to automate the CS selection for mass

minimization while satisfying design constraints. The results of the LBM indicated that a 35% mass reduction in steel structures could lead to a 5% reduction in total lifecycle carbon emissions [25]. Wang et al. (2005) applied shape optimization to design structures with minimal life cycle costs and environmental impacts, using energy consumption as an environmental parameter [26]. Moreover, research has demonstrated that building shape significantly influences energy efficiency. For example, rectangular or trapezoidal shapes often outperform others in minimizing energy use and costs while maintaining structural integrity. Most MOO problems balance embodied carbon emissions against material costs and, thus, illustrate the trade-offs between environmental and economic factors. Schwartz et al. optimized Life Cycle Carbon Footprint (LCCF) and Life Cycle Cost (LCC) for a refurbished housing complex, showing that environmentally optimal solutions often align with cost-effective ones [27].

Although significant efforts have been made to integrate LCA into SO, research on steel-framed structures remains limited, with studies predominantly focusing on composite or reinforced concrete systems [28]. This paper aims to address this research gap by incorporating LCA into the optimization design of steel structures, encompassing manufacturing, assembly, and end-of-life impacts. Previous research has underlined that in the design of space-frame structures lower steel consumption does not always result in lower carbon emission, but there is a substantial positive correlation between them [29]. Based on these premises, this work develops a MOO framework that integrates environmental and structural performance criteria for the optimum design of steel space and hybrid frame structures to evaluate its effectiveness with respect to material usage and environmental impact. The integrated framework incorporates simultaneous size, shape, and topology optimization including environmental parameters such as Global Warming Potential (GWP) and embodied energy.

This research provides comprehensive insight into the trade-offs between structural performance and environmental impact by using a cradle-to-grave LCA approach. The potential for material savings and reduced CO_2 emissions positions this approach in the realm of sustainable construction. Tools such as parametric design software utilizing Visual Programming Language (VPL) and integrated derivative-free optimization Multi-Objective Evolutionary Algorithms (MOEAs) expedite hybrid approaches, which have already proven effective in allowing designers to efficiently explore highly complex trade-offs [30]. These tools address the current challenge of achieving seamless integration between parametric design and LCA in early design stages. In summary, this paper aims to accomplish three primary objectives: *(i)* to develop an easy-to-use, integrated framework based on parametric modelling within commercial software for preliminary design evaluations; *(ii)* to demonstrate the framework's applicability and adaptability across different material types via simple case studies of space-frame structures; *(iii)* to investigate the viability of design solutions that concurrently minimize total embodied energy and material consumption. The paper is organized as follows: Section 2 delineates the methodology for the optimal design of space-frame structures while Section 3 illustrates two case studies to demonstrate the practicality of the proposed framework. Finally, Section 4 provides concluding remarks.

LCA, as defined in refs. [6] - [7], evaluates the full life cycle impact of a generic product, activity, or service across several impact categories including, but not limited to, carbon footprint, water depletion, eutrophication, and toxicity. An LCA comprises four primary stages: (i) goal and scope definition, (ii) inventory analysis (LCI), (iii) impact assessment (LCIA) and (iv) interpretation. In the AEC field, LCA approach is defined by European Standards EN 15978:2011[31] and EN 15804:2012+A2:2019 [32]. Specifically, ref. [31] details the calculation methods, based on LCA and other quantified environmental information, to assess the environmental performance of a building, and provides guidelines for reporting and communicating the assessment outcomes. On the other hand, ref. [32] serves as a widely adopted global standard for generating Environmental Product Declarations (EPD) for construction products. It establishes core Product Category Rules (PCR) for direct assessment of construction products, and can also serve as a basis for developing more specific PCRs for individual product categories. According to ref. [31], information on building products is requisite for the evaluation at the building level, for which EPDs constitute a significant source. The modular framework of buildings life cycle stages is delineated in **Table 1**. The product stage is described in modules A1 to A3, encompassing raw materials extraction (A1), resource transportation to manufacturing (A2), and construction goods production (A3). These modules are considered "cradle-to-gate" within system

boundaries. Material and equipment transport to the construction site (A4 and A5) and construction itself (A5) are incorporated in the construction process stages. The use stage (B1 to B7) covers the period from construction completion to building deconstruction, including usage of building products and services (B1), maintenance (B2), repair (B3), replacement (B4), and refurbishment (B5). The replacement module (B4) comprises the steps for replacing a building component at the end of its service life, restoring initial quality. Repair (B3) entails replacing a damaged component portion, while B4 pertains to the replacement of a whole component. Refurbishment (B5) constitutes a major alteration of a building section to enhance overall technical performance. Energy and water consumed during the use stage are accounted for in modules B6 and B7. The end-of-life stage (C1-C4) addresses waste processing (C3), disposal (C4), waste transport (C2), and deconstruction (C1). Environmental burdens and benefits of reuse, recovery, or recycling are measured in module D. Environmental effects from modules A1 to A3, C1 to C4, and D must be assessed in all EPDs using prescribed indicators, as stated in ref. [32]. These indicators are categorized into resource usage (input-related) and environmental consequences (output-related). Each life cycle module must consider the core indicators: GWP measured in kg CO_2-equivalent emissions and embodied energy, defined as the total energy consumed during production, construction, and end-of-life stages.

Table 1. Building Assessment Information.

Building Assessment Information																								
Building LC info																			Supplementary info beyond LC					
Product Stage (A1-3)			Construction Stage (A4-5)		Use Stage (B1-7)									End of Life (C1-4)				Benefits and loads beyond system boundary (D)					
A1. Raw material Supply	A2. Transport	A3. Manufacturing	A4. Transport	A5. Construction process	B1. Use	B2. Maintenance	B3. Repair	B4. Replacement	B5. Refurbishment	B6.1. Regulated energy of building integrated system	B6.2. Non-regulated energy of building integrated system	B6.3. Non-regulated energy of building non-integrated system	B7. Operational water use	C1. Deconstruction/Demolition	C2. Transport	C3. Waste Processing	C4. Disposal	D1. Potential for reuse, recovery or recycling	D2. Exported utilities					

2 Methodology

The proposed methodology for the optimal design of efficient and sustainable space-frame structures is based on an integrated approach that combines LCA and SO within a MOO framework. Such a framework balances structural efficiency, environmental impact reduction, and practical feasibility, leveraging a Pareto-based approach to navigate conflicting objectives. The simultaneous optimization of size, shape, and topology provides a comprehensive design strategy that overcomes the inherent limitations of individual optimization approaches. The methodology, in fact, fosters seamless integration across design phases and enables minimization of material consumption while ensuring adherence to strength and stability criteria.

The optimization framework in this contribution is fully parametric and operates within a VPL environment, leveraging the functionalities of specialized components. Specifically, Grasshopper (GH) for Rhinoceros 3D® (Rhino3D) software defines the geometric spatial model through nodal coordinates and element connectivity. The Karamba3D[33] plug-in performs the Finite Element Analysis (FEA) and the Octopus plug-in identifies and selects Pareto-optimal design solutions. This automation offers several significant advantages. Firstly, its inherent flexibility allows easy modification of input

parameters, including geometric definitions, material constitutive properties, and loading conditions. This adaptability enables the rapid exploration of the design domain and the efficient evaluation of multiple design alternatives. Moreover, it facilitates sensitivity analysis, which provides valuable insights into the influence of input parameters on both structural performance and environmental impact. Finally, when integrated with advanced optimization algorithms, the parametric model enables a systematic and computationally efficient search for globally optimal designs while substantially mitigating the computational burden associated with complex system optimization.

The framework employs a multi-objective strategy, wherein mass minimization and sustainability objectives, such as CO_2 emissions, are simultaneously addressed within a unified optimization formulation. Penalty functions, based on constraint violation metrics, enforce code-based structural limitations by penalizing non-compliant solutions, thereby discouraging the selection of infeasible designs. These penalties encompass axial force limits, bending moment resistance, buckling safety, and serviceability conditions to ensure compliance with relevant national and European regulations. The computational workflow iteratively explores and refines feasible solutions by rejecting sub-optimal configurations to preserve structural stability and convergence. The proposed optimization framework focuses on ordinary service-life loading conditions typically considered during the preliminary design stage. Accidental actions, such as seismic events, fire scenarios, or man-made hazards, are not explicitly incorporated at this stage and are intended to be addressed through subsequent detailed design and verification phases. Applications to real-world case studies demonstrate the feasibility and adaptability of the proposed methodology to different scenarios, revealing its effectiveness in identifying efficient and sustainable design solutions.

2.1 Optimization Problem Formulation

In this study, the SO problem is framed as a Multi-Objective Optimization (MOO) problem, simultaneously addressing two conflicting objectives: minimizing structural mass and reducing environmental impact. The rationale for these competing objectives stems from the following considerations. Minimizing structural mass typically yields lighter structures, which is advantageous for reducing material consumption and associated costs. However, reduction of the cross-section sizes may necessitate the adoption of higher-grade materials (such as high-strength steel) to accommodate the increased stresses per unit area and satisfy structural performance requirements. Lightweight, high-performance materials such as advanced alloys or carbon fiber composites, in turn, exhibit larger environmental burdens with embodied energy and CO_2 emissions (due to energy-intensive extraction, fabrication, and transportation processes), significantly higher than those of conventional steel or timber. Accordingly, structural mass and environmental impact are simultaneously minimized in the optimization process described herein.

As a preliminary step, the general form of the single-objective optimization problem is presented:

$$\begin{aligned} &\min_{x} f(x) \\ &s.t. \mathrm{g}_k(x) \le 0, k = 1,2,3,\cdots,\mathrm{s} \\ &h_q(x) = 0, q = 1,2,3,\cdots,l \end{aligned} \tag{1}$$

where $g_k(\mathbf{x})$ represents inequality constraint functions (e.g., buckling resistance, maximum allowable deflection, and stress limitations), $h_q(\mathbf{x})$ represents equality constraint functions (such as force equilibrium conditions), and $\mathbf{x}$ is the vector of design variables:

$$x = [x_1, x_2 \ldots, x_n] \tag{2}$$

which, depending on the specific case study, may include CS areas, material properties, element and node locations and connectivity.

The mass function is formulated as:

where N is the total number of elements in the structural system;

$$f_m(x) = \sum_{i=1}^{n} \rho_i A_i L_i \quad (3)$$

ρ_i, A_i and L_i are the material density, cross-section area, and length of the i^{th} element, respectively. This formulation accommodates heterogeneous material densities across the elements of the structural system to enable the optimization of hybrid solutions.

Since the minimization of the environmental impact is included in this study, a second function is defined as:

$$f_{GWP}(x) = \sum_{i=1}^{n} GWPP_i m_i \quad (4)$$

GWP_i is the GWP coefficient of the material used for the i^{th} element, expressed in kg CO_2 equivalent emissions, and m_i is the mass of the i^{th} element.

Considering mass minimization only, the OF for a space-frame structure can be further refined by explicitly considering the individual contributions of beam-column elements and nodes, as follows:

$$OF_1 = \min f_m(x) = \left[\phi \sum_{i=1}^{n} Q_i A_i L_i + \phi_2 \sum_{j=1}^{M} M_{nodj} \right] \quad (5)$$

where M is the total number of node connections and $M_{nod,j}$ is the mass of the j^{th} node.

Two penalty functions (ϕ_1 and ϕ_2) are employed to penalize infeasible solutions. The penalty term increases the value of the objective function as the constraints are violated, effectively converting the constrained optimization problem into an unconstrained one.

Focusing on steel frame structures, Eurocode 3 [34] prescriptions are used to ensure the feasibility of the design solutions. For the i^{th} element, the following local performance check for combined bending and axial compression action is enforced based on element-specific parameters:

$$\frac{N_{Ed,i}}{\chi_{y,i} N_{Rk,i} / \gamma_{Mi}} + k_{yy,i} \frac{M_{y,Ed,i}}{\chi_{LT,i} M_{y,Rk,i} / \gamma_{Mi}} + k_{yz,i} \frac{M_{z,Ed,i}}{M_{z,Rk,i} / \gamma_{Mi}} \leq 1 \quad (6)$$

where $N_{Rk,i}$, $M_{y,Rk,i}$ and $M_{z,Rk,i}$ represent the characteristic resistance values of the axial force and the bending moments about the y and z axis along the member, respectively; and γ_{Mi} is the partial factor of the element material; $k_{yy,i}$ and $k_{yz,i}$ are the interaction factors; $\chi_{y,i}$ is reduction factor due to flexural buckling; $\chi_{LT,i}$ is the reduction factor due to lateral torsional buckling.

Accordingly, this local constraint is applied as a penalty function ϕ_1 within the OF to address non-compliant elements that experience buckling instability:

$$\phi_1 = 1 + n_k K_1 \quad (7)$$

where n_k is the number of structural members violating the performance constraints, and K_1=1.1 imposes a 10% penalty per failing member.

The second function (ϕ_2) penalizes solutions that result in structural systems with an excessively large number of connections, as follows:

$$\phi_2 = MK_2 \quad (8)$$

where K_2 =1.1 applies a 10% penalty to all nodes within the structural system.

Similarly to mass minimization in Eq.(5), the GWP coefficients, representing CO_2 emissions, can be expressed by considering the separate contribution of beam and column elements ($GWP_{b/c}^{tot}$), and nodes (GWP_{nod}^{tot}), as follows:

$$OF_2 = min f_{GWP}(x) = min \left[\phi_1 \phi_3 GWP_{b/c}^{tot} + \phi_2 \sum_{j=1}^{M} M_{nod,j} GWP_{nod}^{tot} \right] \quad (9)$$

In Eq.(9), an additional penalty function is added to meet the Serviceability Limit State (SLS) restriction, which yields:

$$\phi_3 = 1 + \left(\delta_{max} - \delta_k\right) \tag{10}$$

where δ_{max} is the maximum allowable deflection, as specified in refs. [34] and [35]; δ_k is the actual deflection of the structural configuration at the current iteration. If deflections exceed δ_{max}, the penalty increases.

Finally, OF_1 in Eq.(5) and OF_2 in Eq.(9) are combined into a MOO formulation, as follows:

$$OF_{1,2} = min\left[\phi_1\phi_3\sum_{i=1}^{N} Q_i A_i L_I \left(1+GWP_{b/c}^{tot}\right) + \phi_2\sum_{j=1}^{M} M_{nod,j}\left(1+GWP_{nod}^{tot}\right)\right] \tag{11}$$

Explicitly, in this formulation size optimization is achieved by adjusting element CS areas; shape is refined through modulation of node locations; topology is optimized by modifying element connectivity. All these optimizations are performed while enforcing inequality constraint functions via penalties such as those based on member resistance and deflection limits.

2.2 Optimization Framework

The optimization framework proposed herein is based on computational methods for optimization routines within a VPL environment. An explanatory flowchart is presented in **Fig. 1**. First, a parametric digital model is generated using the graphic algorithm editor Grasshopper (GH) for Rhino3D via a Python script, which aids user interaction with the 3D system. Based on this initial geometry, the structural model including elements, applied loads and boundary conditions, is directly characterized using the Karamba3D add-on [33]. This facilitates structural checks in agreement with Eurocode.

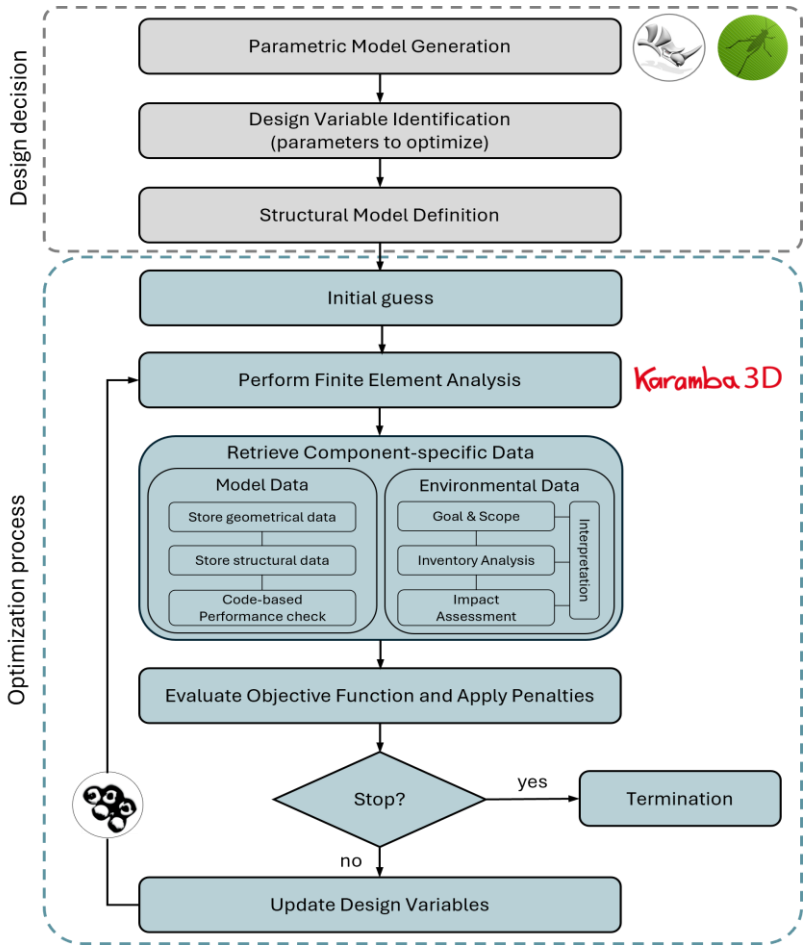

Fig. 1. Flowchart of the optimization framework.

Appropriate design variables, namely the parameters optimized through the whole process, are identified. Depending on the optimization type and the specific case study, design variables can include one of the following parameters or a combination thereof: cross-section sizes of structural members or components (size optimization), nodal coordinates of the structure (shape optimization), and node connectivity (topology optimization). An initial guess for these parameters initiates the optimization process. At each optimization iteration, a linear static FEA is conducted in Karamba3D on the specific configuration, and relevant performance parameters are recorded. These results are used to verify the load-bearing capacity, stability, and safety of the structural configurations against Eurocode 3-5 and Italian technical code (NTC) criteria [34], [35], [36].

Concurrently, environmental impact is quantified in terms of GWP in kg CO_2 equivalent emissions, with LCA performed according to the European standard [32] for comprehensive sustainability evaluation.

Building-level LCA is essential for quantifying total environmental impact, and its use for comparing building environmental performance is increasingly common. Consequently, various LCA software programs exist; nonetheless, it is essential to recognize the possible impact of different software and databases on outcomes [37]. The LCA is conducted herein without reliance on external software. Instead, a Life Cycle Inventory (LCI) is generated by combining quantities (e.g., mass, length, element cross-section) collected from GH with available environmental impact data. Product and producer-specific EPDs are preferred data sources. Where unavailable, generic LCA datasets with broader applicability can be used.

Notably, this study focuses on the GWP impact category only. For each component or material, the derived quantities are multiplied by the GWP value provided by the corresponding dataset. Specific details on the GWP impact assessment are presented in Section 3. The goal and scope phase is executed once the product system, functional unit, system boundary, and data requirements are established. Material and process information is matched and linked with environmental data of the processes contained within the system boundary. This enables the automated generation of an LCI, whose emissions outputs are then converted into impact indicators as required during the LCIA stage (**Fig. 1**).

Then, the objective function in Eq. (11) is evaluated by integrating LCA estimates and structural model data. Finally, the single optimization cycle is driven by the Strength Pareto Evolutionary Algorithm II (SPEA-II) [38] within the Octopus plug-in [39]. This derivative-free MOEA Graphical User Interface (GUI), integrated within the GH-VPL environment, enables the exploration of multiple design solutions compliant with Eurocode 3 and Eurocode 5 constraints. The algorithm employs a penalty-based approach and Tournament Selection for the selection process. Mutation and crossover probabilities are set to 0.2 and 0.8, respectively. The population size and number of maximum iterations are specialized for the specific case study. The design variables are iteratively adjusted to optimize the objective function while satisfying the constraint defined in Eq. (6). The algorithm continues iterating beyond the identification of feasible solutions satisfying this constraint in order to refine the Pareto front. The optimization process terminates when either the predefined maximum iteration count is reached or a convergence threshold of 0.1% is met.

3 Case Studies

To demonstrate the effectiveness of integrating LCA into structural optimization, two case studies are presented: (i) a steel space-frame and (ii) a hybrid steel-timber frame structure. The steel frame solution is optimized for mass minimization only, utilizing a single-objective function (OF_1) in Eq. (5). On the other hand, the hybrid solution integrates an additional objective function (OF_2) aimed at mitigating environmental impact via CO_2 footprint minimization, resulting in the MOO formulation with $OF_{1,2}$ expressed in Eq. (11). The outcomes of this study provide valuable insights into how a balance between structural efficiency and sustainability can be achieved. Size, shape, and topology are simultaneously optimized in the case studies. By comparing the optimized steel space-frame with the hybrid steel-timber solution, the study highlights the potential for significant reductions in environmental impact through the strategic integration of timber elements, while maintaining or enhancing structural performance. The MOEA's ability to handle multiple design objectives and generate a set of Pareto-optimal solutions enables designers to make informed decisions based on specific project requirements and sustainability goals.

3.1 Case study 1

The first case study examines a double-layered steel space-frame structural system with a total span length of 60 m in the x direction (Lx) and of 30 m span in the y direction (Ly). Case Study 1 is conceived as a preliminary benchmark aimed at assessing the impact of clustering strategies under mass minimization only, prior to introducing environmental objectives in the multi-objective framework. Modularity and repetition are elected as primary design considerations to ensure a structurally efficient and cost-effective solution. The structural arrangement and member alignments follow a systematic configuration, wherein diagonal components connect the top and bottom chord planes to generate a three-dimensional framework. The truss overall height (H) is initially set to 4 m, striking a balance between efficient material usage and structural rigidity. Joints are evenly spaced to facilitate uniform load distribution and mitigate localized stress concentrations. The initial geometry is parameterized within the GH-VPL environment using the IronPython component [40], which enables real-time variation of the design variables throughout the optimization process (**Fig. 2(a)**). Specifically, each component is adjustable using a number slider component available in GH (**Fig. 2(b)**) in terms of H, number of elements in the x and y directions (div_x, div_y), and spacing between nodes in both horizontal directions (Δx, Δy). Here, Δ_x and Δ_y denote the nodal spacing in the x and y directions, respectively, and are dependent parameters determined by the overall span and the selected values of div_x and div_y. The labels of the IronPython component in **Fig. 2(a)** describe the following groups: (i) Up Chord defines the constituent lines of the upper layer; (ii) Low Chord defines the constituent lines of lower layer; (iii) Tot_Diag comprises all connective diagonals between the two layers; (iv) Tot Nods includes all nodes in the structural system; (v) Supports Corners consists of the four corner nodes defying the support locations. Additionally, (vi, vii, viii) Load_Gr1, Load_Gr2, Load_Gr3, Load_Gr4 represent beam clusters for manually designating influence areas for load application.

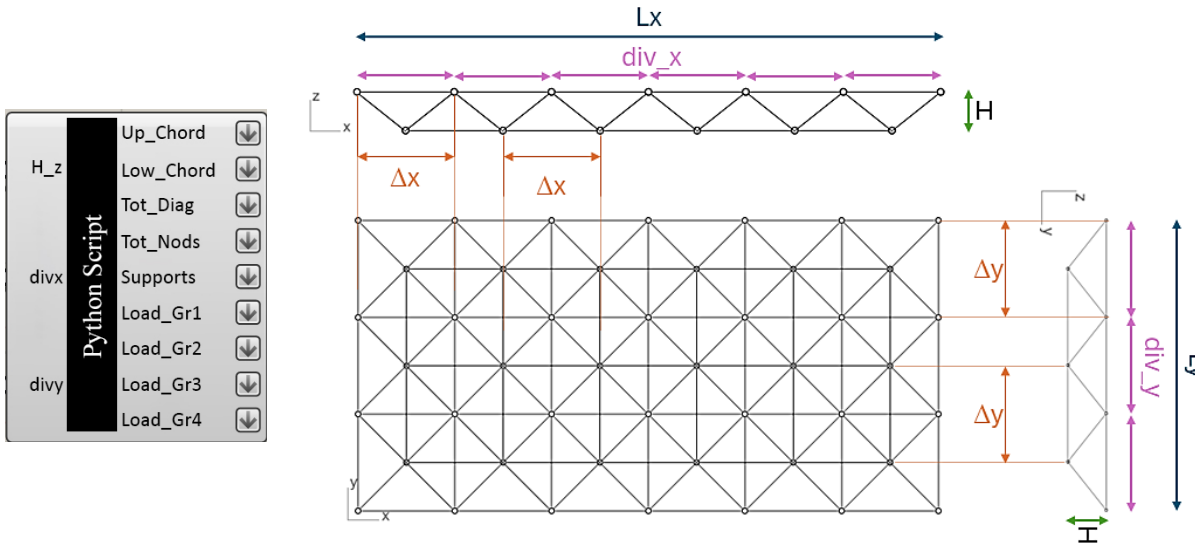

(a) IronPython component (b) IronPython geometry output - Case Study 1

Fig. 2. GH-Python definition

The design variables are bounded by the following preliminary dimensioning rules. The upper bound for H is determined by assuming a height-to-span ratio (H/L) of 1/15, where L is the larger span of the structure (Lx in this case). This relationship aligns with generalized best practice and recommended limits for space-frames (e.g., [41]), balancing stiffness and material efficiency. A lower bound of 0.5 m is imposed for H to ensure constructability and provide sufficient depth to resist bending and deflection. The span of the frame structure (denoted as Δ) is determined by the number of subdivisions in the x and y directions and the overall dimensions of the space-frame. Therefore, Δ is not an explicitly independent design variable but rather a dependent parameter. The number of subdivisions div_x and div_y are the design variables and are constrained within $L_x/\Delta_{max} \leq div_x \leq L_x/\Delta_{min}$ and $L_y/\Delta_{max} \leq div_y \leq L_y/\Delta_{min}$, respectively, where Δ_{max} and Δ_{min} represent the

minimum and maximum allowable spans. The values for Δ are implicitly defined by the chosen ranges for div_x and div_y, which effectively limit the length of the beam elements to be within a desired range. In this case, the minimum and maximum dimensions are assumed to be 1 m and 10 m, respectively.

Spherical joints, with a pre-defined diameter of 0.30 m, consistent with common structural design practice, are employed to connect the structural elements. These joints are excluded from the optimization process as design variables. For these standardized components, in fact, their quantity is considered a more critical design parameter than their specific typology.

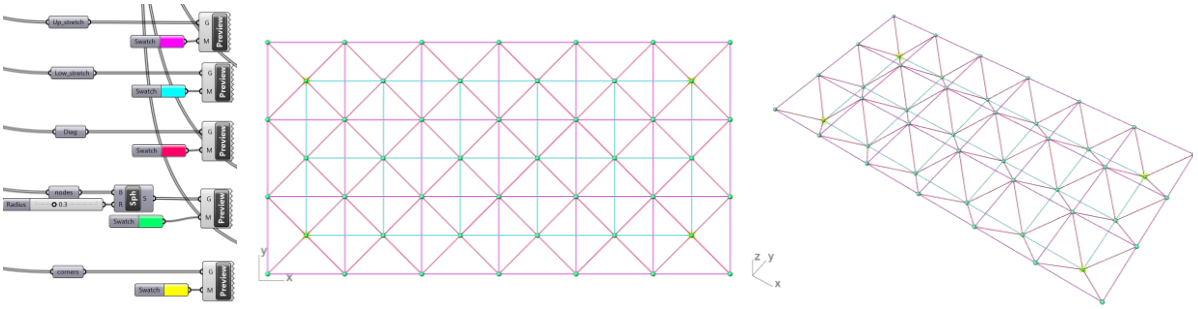

Fig. 3. Geometric element characterization in GH-VPL for Case study 1.

Upon generation of the parametric geometry, the lines are converted into beam elements. The transition from the geometrical model to the FE model is performed using the Karamba3D solver in the GH environment. The structure is composed exclusively of Circular Hollow Section (CHS) steel profiles, which are selected for their high strength-to-weight ratio and suitability for long-span applications. The overall structural system is constructed from S355 steel grade with a material density of 7,850 kg/m³. To ensure constructability, cross-sections are selected from predefined standard profiles, excluding slender sections vulnerable to buckling. Although Class 4 steel sections are permitted by Eurocode 3 for specific applications, they are not considered in this study due to their higher susceptibility to local buckling and the additional modeling complexity required at the preliminary design stage.

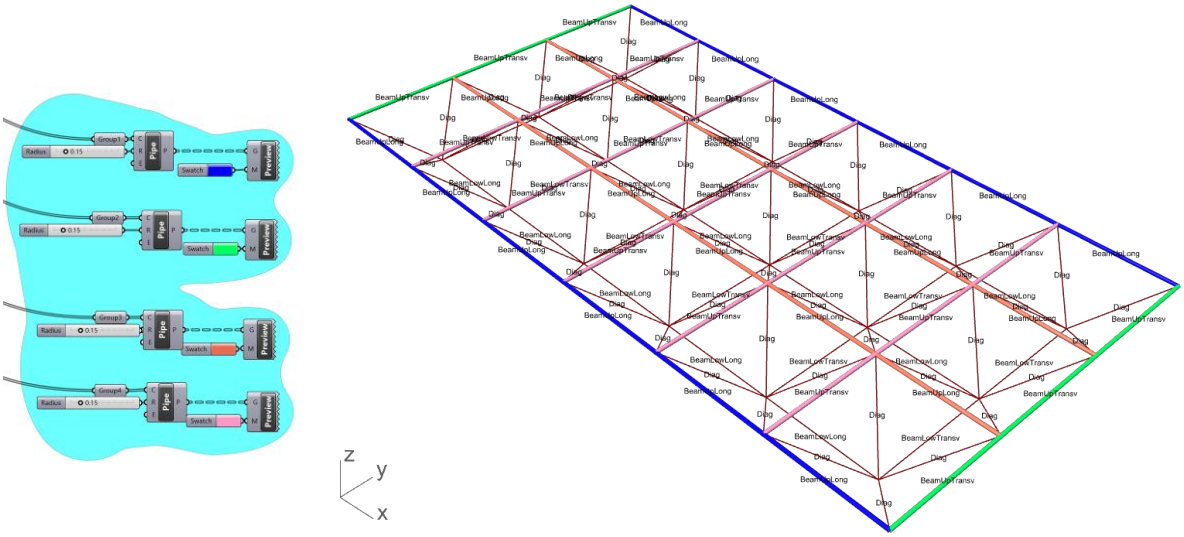

(a) GH-output script (b) Loaded frame clustered by colors

Fig. 4. Load element assignment for Case study 1.

The available Karamba3D catalogue of CSs is employed. The initial list of 221 European CHS is transferred to an .xls file, from which a limited range is chosen. From this catalogue, the EN10219-2 CHS standard sections are considered, resulting in a total of 177 sections. The rationale for this selection is to use only Classes 1, 2, and 3 sections [34], thus excluding Class 4 CSs where local buckling would occur before yielding. Sections satisfying the relationship $D/t \geq 90\epsilon^2$ are omitted, with D and t being

the outer diameter and wall thickness, respectively, and ϵ being contingent on the steel grade (0.81 for S355). As a starting guess, all beams share the same CHS profile, which is then iteratively adjusted throughout the optimization process.

The Karamba 3D Support component is used to define four fixed supports at the corners of the lower layer (yellow points in **Fig. 3**). The Beam-Joints component is employed to generate and identify joints, maintaining a record of geometric connectivity. This component also defines hinged connections at the element ends, effectively converting beam elements into truss-like elements.

Loads are applied as distributed forces on beams of the upper layer, with influence areas calculated to ensure accurate load distribution. The corresponding clusters labelled as *Load_Gr1, Load_Gr2, Load_Gr3*, and *Load_Gr4* in the IronPython geometry definition shown in **Fig. 2(a)** are detailed in the geometric output presented in **Fig. 4(b).**

In this initial optimization phase, only gravity loads — specifically, dead loads, live loads, and snow loads — are considered. This approach is justified by the fact that gravity loads often play a dominant role in the initial design stages of space-frame structures.

This dominance makes gravity loads a primary driver in determining the overall structural form, member sizing, and material distribution. Optimizing for gravity loads effectively establishes a robust load-carrying system, defining the primary load paths and influencing the overall structural layout. The resulting design often provides a strong foundation for subsequent refinement. It is crucial to emphasize that while lateral loads are excluded from this initial optimization, the designs resulting from this phase must be rigorously verified post-optimization against all other relevant load combinations (including wind and seismic loads). This verification process ensures full compliance with code-based requirements and guarantees the safety and performance of the final design under all anticipated loading conditions. Moreover, focusing on gravity loads in this initial phase offers significant computational advantages. By addressing a reduced optimization problem, the design space can be explored more rapidly, leading to the identification of promising initial designs with reduced computational effort.

This simplification is also necessitated by the limitations of the Karamba-FE solver employed in this study, which can only process one load combination at a time. Thus the following Ultimate Limit State (ULS) combination, specialized to include only dominant gravity loads, is employed in accordance with Eurocode [42] and NTC2018 [36]:

$$\gamma_{G1}G_1 + \gamma_{G2}G_2 + \gamma_{Q1}G_{k1} + \gamma_{Q2}\psi_{02}Q_{k2} + \gamma_{Q3}\psi_{03}Q_{k3} + ... \quad (12)$$

in which, G_1 is the dead load and G_2 the permanent non-structural load from the corrugated sheeting; Q_{kj} are the variable loads; ψ_{0j} are the combination coefficients, and γ the partial safety factors. The gravitational forces applied to the case-study are detailed in **Table 2**.

Table 2. Gravity loads applied in Case Study 1.

Load Type	Load Value	γ
Dead load (G_1)	VPL self-computed [kN]	1.3
Corrugated Sheet load (G_2)	1.57 kN/m^2	1.5
Snow load (Q_1)	1.23 kN/m^2	1.5

The structure adheres to Eurocode 3, so that axial force, bending moment, buckling resistance, and deflections remain within acceptable thresholds. With reference to the constraint function in Eq. (6), the terms for steel CHS profiles are specialized as follows. The characteristic axial resistance for the i^{th} element is defined as:

$$N_{Rk,i} = f_y A_i \quad (13)$$

where f_y is the yield strength of steel and A_i is the cross-sectional area. For CHS profiles, the characteristic bending moment resistance about the relevant y or z axis along the member is calculated as:

$$N_{R_k,i} = W_y f_y \quad (14)$$

where W_i is the appropriate section modulus depending on the Class of the CS.

Finally, the Demand/Capacity Ratio (DCR) expressed in Eq. (6) is used to evaluate the structural efficiency of each member of the structural system.

Serviceability limits for deflection are also enforced to ensure acceptable deformations:

$$\partial \leq \partial_{max} \quad (15)$$

where ∂ is the deflection value computed at each iteration of the optimization process, and $\partial_{\max}$ is the maximum allowable deflection defined by serviceability criteria [34]. Specifically, $\partial_{\max} = \mathrm{L}/200$ if roofs without brittle elements are assumed, where L is the relevant span.

Table 3. Design variables for Case Study 1.

Description	xi	ULbounds
Roof Height	x1 = H	[0.5, L/15] [m]
Total span division on x-axis	x2 = divx	[6, 60] (integer)
Total span division on y-axis	x3 = divy	[3, 30] (integer)
CHS up. chord, low. Chord, diag. (X-Y axis)	x[4,8]	[0, 176] (solver index)

Following the definition of all elements and parameters for the FEA, the OF is implemented to minimize structural mass. To enhance material efficiency and reduce design variable dimensionality, frame elements are systematically categorised into predefined groups (i.e., clusters) based on similar load distributions to optimize their cross-sectional areas. By grouping elements with comparable stress conditions and load distributions, the optimization process avoids redundant evaluations of individual components, leading to more efficient material allocation and a reduced search space. This clustering strategy leverages the principle that elements subjected to similar loading conditions can be assigned identical cross-sectional properties without compromising structural integrity.

In this case study, three distinct clustering strategies are examined to assess their impact on the optimization results: (a) uniform CS assignment for all frame elements (resulting in a single design variable for CS selection); (b) component-based CS assignments for upper chord, lower chord, and diagonal elements (resulting in three design variables); (c) strategy with directional refinement of separate CSs for longitudinal and transverse members (resulting in five design variables). The design variables (x_i) along with their corresponding upper and lower bounds (UL_{bounds}) are summarized in **Table 3**. These bounds are crucial as they define the feasible design space, ensuring that the optimization process identifies only structurally viable and manufacturable solutions. As previously discussed, the bounds are derived from preliminary dimensioning rules and constructability considerations.

Table 4. Algorithm setting for GA -SPEAII in Case Study 1.

Parameters	Settings
Max Number of Iterations	200
Population Size	200
Mutation Probability	0.2
Crossover	0.8
Threshold 0.001	0.001
Penalty Functions	$\phi 1$, $\phi 2$
Algorithm Integration	SPEA-II

The structure is topologically optimized by adjusting both its height and the number of elements and nodes along the two directions (Lx and Ly). In addition to TO, also shape and size optimization are conducted, enabling the simultaneous optimization of beam element CSs. The three optimization approaches are executed employing the SPEAII algorithm within the Octopus plug-in for GH, with the algorithm settings provided in **Table 4**. By applying the OF_1 in Eq. (5), the optimization algorithm evaluates multiple structural arrangements and identifies the most effective configurations in terms of structural efficiency and material savings. For the three clustering strategies under consideration, the optimization yields the following results for structural mass: M_a = 255.1 ton for cluster (a), M_b = 172.3

ton for cluster (b), and M_c = 158.9 ton for cluster (c). The outcomes are illustrated in **Fig. 5** and **Fig. 6**, where different line colors denote different CSs (thus, different clusters).

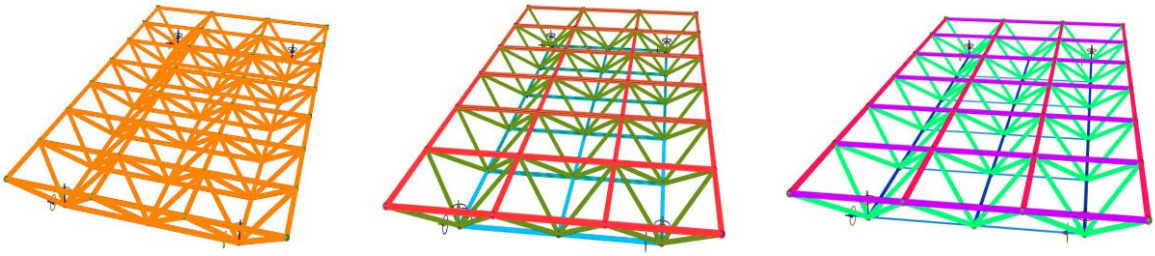

(a) Optimal configuration *(a)* (b) Optimal configuration (*b*) (c) Optimal configuration (*c*)

Fig. 5. 3D views of the optimized configurations for the three clustering strategies in Case Study 1.

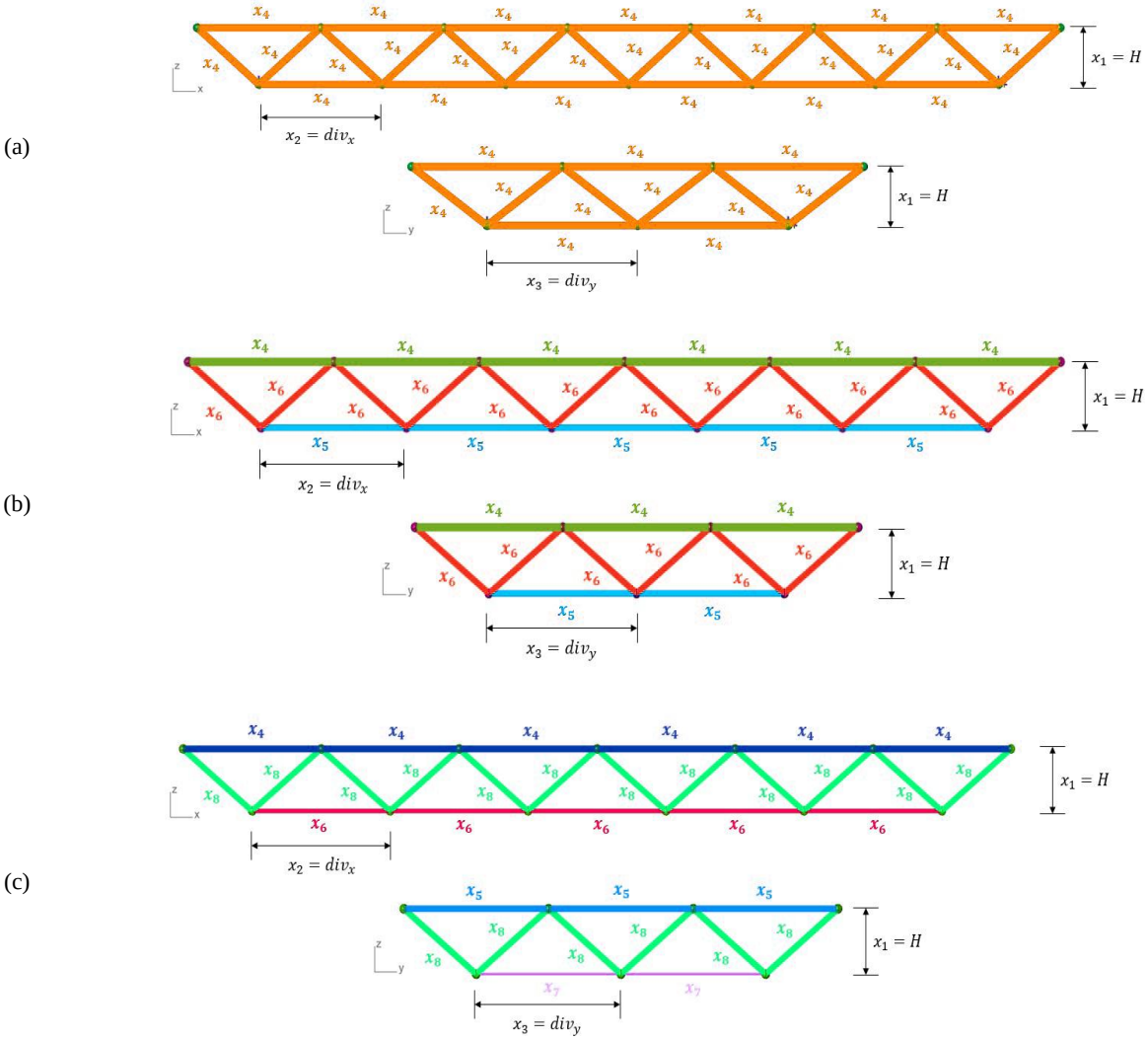

Fig. 6. Longitudinal and transverse CS of the optimized configurations (a), (b) and (c) in Case Study 1 with specifications of the corresponding design variables.

The results indicate that implementing a uniform cross-section across the entire structure would necessitate dimensioning all members to withstand the peak stresses experienced by the most heavily loaded component. This strategy largely simplifies the optimization problem but results in sub-optimal material utilization with a significant increase in overall structural mass and compromised material efficiency. Conversely, allowing the optimization algorithm to assign distinct cross-sections based on

different member clusters enables the definition of a minimal-weight structure, albeit with increased design complexity depending on the number of clusters assigned. The post-optimization values for the design variable listed in **Table 3** are summarized in **Table 5**.

Table 5. Optimal values of design variables for Case Study 1.

Variables	(a)	(b)	(c)
x1 = H [m]	3.9	4	4
x2 = divx [-]	7	6	6
x3 = divy [-]	3	3	3
x4 = CHS [mm]	457x12.5*	508x12*	508x12*
x5 = CHS [mm]	-	219.1x12*	355.6x10*
x6 = CHS [mm]	-	323.9x10*	323.9x12*
x7 = CHS [mm]	-	-	168.3x5*
x8 = CHS [mm]	-	-	323.9x10*

Compared to solution (a), the element total weight in solution (b) is reduced by approximately 32%, with a further 8% reduction achieved in solution (c) through minor refinements. This progressive reduction highlights the significant impact of clustering strategies on material efficiency.

For all three conditions, the convergence to the optimal solution is attained rapidly at the first iteration with optimal height (H) of 4.0 m, $div_x = 6$ and $div_y = 3$. This results in a modular span (Δ) of 10 m. The optimal configurations, characterized by a reduced number of connections, are favored by the optimization algorithm when larger CSs are assigned to each structural element.

The evolution of the optimal solution during the optimization routines can be observed in **Fig. 7**, which illustrates the iteration histories of the objective function defined in Eq.(5), the total mass function, and the constraint violation proportion (i.e., the estimated percentage of unfeasible individuals) with respect to the number of iterations required. It should be noted that the objective function includes penalty terms to enforce feasibility constraints, and therefore does not exactly coincide with the total structural mass, particularly during the early iterations and for clustering strategies characterized by higher constraint violations. **Fig. 7(c)** indicates that the optimization algorithm generates a large number of unfeasible individuals at each iteration to enhance the exploration of the whole design space. The observed rapid drop of the OF in **Fig. 7(a)** trend indicates the algorithm's efficiency in navigating the design space and identifying feasible solutions. This rapid decrease, coupled with the stabilization of the constraint violation proportion, suggests that the algorithm effectively balances objective function minimization with constraint satisfaction. The steady convergence of both the OF trend and the constraint violation proportion as well as the limited number of optimization cycles required for all the three design strategies further validates the robustness and efficiency of the proposed optimization process. It is observed that the element lengths determined by the optimizer comply with requirements for on-site assembly and transportability, with a maximum allowable length of 12 meters for transport rods. Considering these factors, in conjunction with the substantial mass reduction achieved, solution (c) is deemed the most effective clustering strategy in balancing material efficiency, structural integrity, and practical constructability. Consequently, its related topology and clustering configuration are adopted in the subsequent case studies.

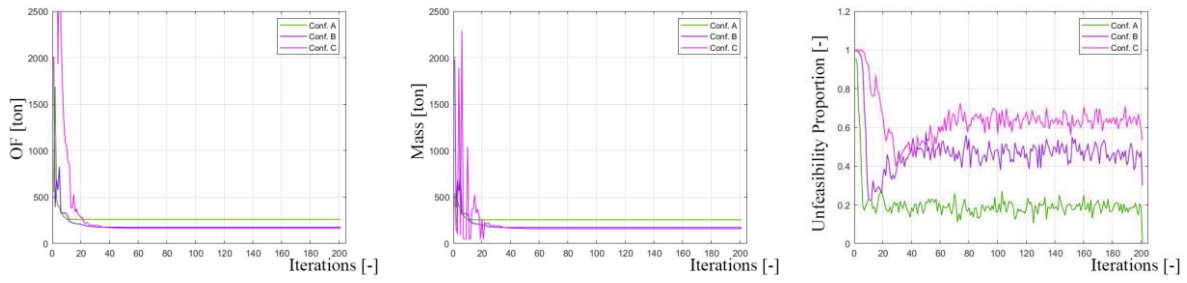

(a) OF (b) Total Mass (c) Unfeasible Solutions

Fig. 7. Iteration histories for the three clustering strategies.

3.2 Case study 2

The second case study investigates the design of a single-story hybrid steel-timber structure with plan dimensions of 60 m x 30 m. This study explores the potential of integrating mass timber elements with steel to achieve a balance between structural efficiency and reduced environmental impact. Numerous comparative LCA studies have consistently demonstrated that structures constructed with Mass Timber Products (MTPs) typically exhibit lower GWP compared to traditional concrete or steel structures. This is primarily attributed to the biogenic carbon storage in timber and the reduced energy consumption during its production. As a result, the utilization of timber has emerged as a viable and effective solution for achieving sustainability goals [43], [44].

The test case system integrates glulam-timber members with steel CHS profiles. This hybrid approach is strategically selected to optimize structural performance, sustainability, and cost-effectiveness. This goal is achieved by leveraging the high stiffness-to-weight ratio of steel profiles while benefiting from the reduced embodied carbon footprint of timber. The structural layout (as illustrated in **Fig. 8**) comprises primary beams and diagonal members, constructed from steel CHS profiles or rectangular timber sections, and glulam columns as vertical supports.

A MOO is performed using the Evolutionary Algorithm (EA) solver to simultaneously minimize structural mass and associated CO_2 equivalent emissions (GWP), in accordance with the methodology outlined in [32]. The $OF_{1,2}$ defined in Eq.(11) is employed for this purpose.

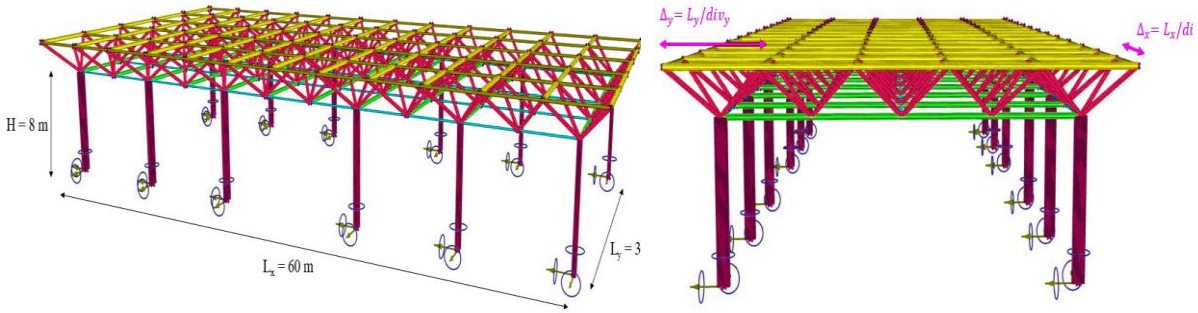

Fig. 8. Hybrid steel-timber structure for Case Study 2.

The structure's design is parameterized following the methodology established in the previous case study. The upper components, which constitute the roof system, are constructed with identical specifications. To accommodate additional vertical supports, 8 m-high columns are positioned symmetrically along the x axis of the frame structure. For the FEA, each structural member is modelled as a beam element using the built-in Karamba 3D - GH solver. The material assignments for this case study are detailed in **Table 6**. The structural system is supported by columns fixed at their base. Connections between elements are modelled as pinned.

Table 6. Material properties adopted in Case Study 2.

Material	Density (kg/m^3)	Yield/Strength parameter (MPa)	Young's Modulus (GPa)
Steel – S355	7850	355	210
Glulam Timber – GL28h	470	28	12

Table 7 summarizes the applied loads on the structural system. The loads are subsequently combined using the ULS defined in Eq. (12). Applied loads are evaluated in agreement with NTC2018 [36] and include permanent structural load (G_1), permanent non-structural load (G_2), maintenance load (Q_1), snow load (Q_2) and wind load (Q_3). It is important to note that, in contrast to Case Study 1, wind loads are explicitly considered in this case. This distinction arises from the fundamental difference in structural topology: Case Study 1 focused on a space-frame truss, primarily simulating a roof structure, where gravity loads were deemed dominant for initial optimization. However, Case Study 2 investigates a complete single-story frame structure, including vertical elements (columns). In frame structures,

wind loads exert significant lateral forces, which must be accounted for to ensure structural stability and integrity. Therefore, wind loads are included in the ULS combination for this case study to accurately represent the loading conditions.

Table 7. Loads applied in Case Study 2.

Load Type	Load Value [kN/m^2]	γ	ψ
Structural Load (G_1)	Solver Self-Computed	-	-
Non-structural Load (G_2)	0.05	1.5	-
Maintenance Load (Q_1)	0.5	1.5	-
Snow Load (Q_2)	1.23	1.5	0.5
Wind Load (Q_3)	Depends on c_p^1, c_e^2	1.5	0.6

[1] Pressure coefficient influenced by the building's design, shape, and positioning relative to wind forces.

[2] Exposure coefficient depending on the ground topography, location, and height of the structure.

CS assignment and clustering for the roof system follow the procedures established in Case Study 1. A typological differentiation is implemented for roof CS selection, allowing the optimization algorithm to choose between open and closed sections. The available cross-section options include: a) Upper and Lower Chords: CHS or IPE sections (steel); b) Diagonals: steel CHS, steel double L-sections, or rectangular timber sections; c) Columns: rectangular timber sections.

The CS assigned to the diagonal members facilitates the evaluation of two distinct scenarios: (i) steel sections and (ii) glulam sections. For clarity, these scenarios are regarded as independent case studies in the following, namely Case study 2.1 (steel diagonals) and Case study 2.2 (timber diagonals), respectively. Class 4 items are removed from the Karamba3D steel CS catalogue. The design variables (x_i) adopted, along with their respective upper and lower bounds (UL_{bounds}), are summarized in **Table 8**.

Table 8. Design variables for Case Study 2.

Description	xi	ULbounds
Roof Height	x1 = H	[1, 3] [m]
Total span division on x-axis	x2 = divx	[6, 40] (integer)
Total span division on y-axis	x3 = divy	[3, 20] (integer)
CS up. and low. chord on x, y dir.	x[4,7]	[0, 170] IPE/CHS (solver index)
Diagonal CS	x8	[0 , 170] CHS/ 2L (solver index, Case study 2.1) [0, 201] CHS/2L/Glulam (solver index, Case study 2.2)
Column CS	x9	[0, 150] Glulam (solver index)

In this second case study, the MOO optimization problem is formulated to simultaneously minimize structural mass (OF_1 in Eq. (5)) and minimize environmental impact (OF_2 in Eq. (9)). The environmental impact for case studies 2.1 and 2.2 is assessed using the LCA framework following the standards [32]. This ensures that the full cradle-to-grave impact of material selections is properly accounted, providing a robust comparison of sustainability metrics. The optimization problem employs the penalty-based $OF_{1,2}$, as defined in Eq. (11) to handle constraints. Structural integrity constraints, enforced through penalty functions, adhere to Eurocode 3 [34] for steel members (Eq. (6)) and Eurocode 5 [35] for timber members.

The characteristic axial resistance of timber members is defined as:

$$N_{Rk,i} = k_{\mathrm{mod}} f_{c,0,k} A_i \quad (16)$$

where k_{mod} is the modification factor for timber strength based on moisture content and load duration; $f_{c,0,k}$ is the characteristic compressive strength of glulam; A_i is the cross-sectional area.

The characteristic bending moment resistance about the relevant axis is calculated as:

$$M_{Rk,i} = k_{\mathrm{mod}} f_{\mathrm{m},k} W_i \quad (17)$$

where $f_{m,k}$ is the characteristic bending strength of glulam and W_i is the appropriate section modulus of the element section.

The shear resistance check for bolted steel-to-timber connections is performed using:

$$F_{v,\mathrm{Rd,j}} = k_{\mathrm{mod}} \cdot \frac{f_{v,k} d^2}{\gamma_{M2}} \quad (18)$$

where $f_{v,k}$ is the characteristic shear strength of timber; d_j is the bolt diameter for the *j-th* connection and γ_{M2} is the partial factor of the timber material. The subscript *j* indicates that the equation is applied individually to each bolted connection in the structure.

To ensure serviceability, deflection constraints are enforced. For steel elements, the maximum allowable deflection is $L/200$, while for timber structures with sensitive materials, this limit is reduced to $L/300$. Given that the frame structure under consideration is a steel-timber hybrid, the more restrictive value is conservatively assumed as the maximum allowable deflection to guarantee serviceability.

To quantify the environmental impact within the optimization framework, LCA data, specifically GWP, are integrated. The GWP is assessed across critical life-cycle stages: Production (A1-3), Installation/Assembly (A5), End-of-Life (C) and potential for recycling/reuse (D). The GWP values for A1-3 are summarized in **Table 9**.

Table 9. LCA data – Stage A1-3

Materials (A1-3)	GWP [$kgCO_2$-eq./ton.]
Closed steel profiles	1125
Open steel profiles	3151.13
Stainless steel screw	4103
Timber elements	-1294.468

The *A5* considers the emissions associated with on-site processes, applying a GWP_{A5} = 0.817 $kgCO_2$ − eq./m exclusively to steel profiles, reflecting the energy required for their assembly. The total GWP_{A5} is obtained by summing the processes related to steel laser cutting, steel laser welding and welding seam (1m). For end-of-life (C) and credits (D), specific scenarios are defined. Steel is assumed to be processed for reuse as primary steel, however, the environmental benefits of a subsequent life cycle are not explicitly included in this analysis. Glulam elements are assumed to undergo incineration with thermal energy recovery, reflecting common end-of-life practices for wood waste. In this case, the corresponding GWP data are (**Table 10**):

Table 10. LCA data – Stage C and D

Materials (C+D)	GWP (C) [$kgCO_2$-eq./ton.]	GWP (D) [$kgCO_2$-eq./ton.]
Closed steel profiles	0.6821	-393
Open steel profiles	0.6821	-393
Stainless steel screw	2.785	-1326
Timber elements	-1606.002	-872.127

The optimization algorithm incorporates GWP data, dynamically adjusting the environmental impact based on the material quantities utilized at each iteration. This approach allows for a comprehensive assessment of the environmental performance of the structure.

Table 11. Algorithm setting for GA -SPEAII in Case Study 2.

Parameters	Settings
Max Number of Iterations	100
Population Size	200
Mutation Probability	0.2
Crossover	0.8
Threshold 0.001	0.001
Penalty Functions	$\phi 1$, $\phi 2$, $\phi 3$
Algorithm Integration	SPEA-II

Following the algorithm configuration detailed in **Table 11**, and utilizing predefined GWP values, the optimization process is executed for the two scenarios (Case Studies 2.1 and 2.2), enabling a comparative analysis of their environmental footprints.

Fig. 9 presents the Pareto-optimal front, which illustrates the trade-offs between structural mass and CO_2 emissions. Two extreme points of the Pareto front and an intermediate design solution, designated as S_1, S_2 and S_3, are selected for detailed evaluation against the Utopia-point (U_p) [45]. The U_p represents an idealized solution in MOO where all objective functions simultaneously achieve their absolute optima. In practice, the optimization algorithm identifies the solution on the Pareto front that minimizes the distance to the U_p, effectively determining the "best compromise" solution. In the case studies under investigation, the Utopia-point solution serves several critical purposes. First, it facilitates the identification of a design solution that optimally balances competing objectives, namely minimizing structural mass and environmental impact. Second, it provides a quantitative basis for comparing the performance of different design alternatives in relation to the ideal solution. Third, it enables the assessment of the proximity of each alternative solution to the ideal U_p, quantifying the degree to which the ideal is achieved. The Utopia point (Up) is defined in the objective space as the ideal reference point Up = (min(OF_1), min(OF_2)), where each objective independently achieves its minimum value. Since this point is generally not feasible, the optimization algorithm identifies the U-point solution as the Pareto-optimal design that minimizes the Euclidean distance to U_p in the normalized objective space. Finally, it supports informed decision-making by providing a clear visualization of the trade-offs and a quantitative measure of the optimality of different design configurations, thereby guiding the selection of structural and material configurations that achieve an optimal balance of sustainability and efficiency. The resulting optimal solutions for Case Study 2.1, which exclusively utilizes steel CHS for the space-frame system, are detailed in **Table 12.**

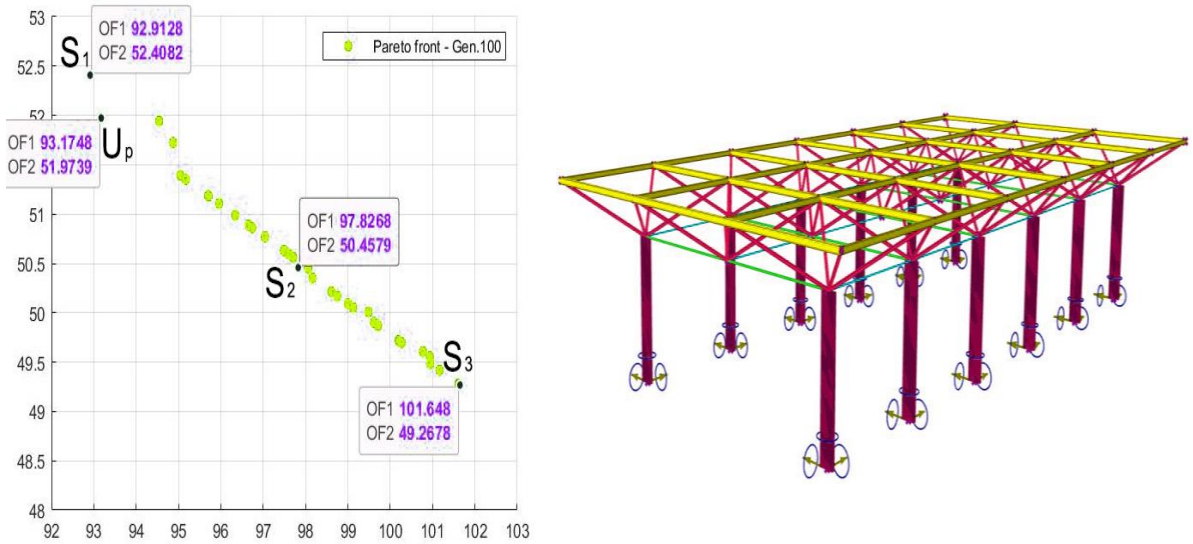

(a) Pareto optimal front (b) Optimal configuration

Fig. 9. Post-optimization Case Study 2.1

In this case study, closed steel sections are preferred for beam clusters due to their enhanced torsional stiffness and structural capacity compared to open sections. This choice is particularly advantageous in space-frame structures where torsional effects might be significant. The optimization algorithm favors designs with fewer modules, specifically a 6x3 configuration (modules in the x and y directions, respectively), is identified to minimize component count, overall structural mass, and embodied emissions. The roof height, consistently converging towards the upper bound of its variable

range at 3 m for all the selected solutions, facilitates a more uniform and efficient stress distribution within the space-frame. Additionally, **Fig. 10** shows that the number of connections and associated GWP remain constant across the four optimized designs, all of which maintain the 6x3 modular division. This indicates that the optimization process primarily focuses on adjusting member sizes and material distribution rather than altering the topological configuration of the space-frame.

Table 12. Optimal values of design variables for case study 2.1.

Parameter	Up	S1	S2	S3
OF1 (Mass)	93.17	92.91	97.83	101.65
OF2 (GWP)	51.97	52.41	50.46	49.27
Height (H) [m]	3	3	3	3
Divisions (x-dir.)	6	6	6	6
Divisions (y-dir.)	3	3	3	3
Up. Chord (Long.)	CHS 355.6x6.3	CHS 406.4x6	CHS 355.6x6.3	CHS 355.6x6.3
Low. Chord (Long.)	CHS 139.7x3	CHS 114.3x2.5	CHS 114.3x2.5	CHS 114.3x2.5
Up. Chord (Transv.)	CHS 406.4x6	CHS 406.4x6	CHS 406.4x6	CHS 406.4x6
Low Chord (Transv.)	CHS 139.7x3	CHS 114.3x3	CHS 139.7x4	CHS 139.7x5
Diagonals	CHS 219.1x5	CHS 219.1x5	CHS 219.1x5	CHS 219.1x5
Columns	GL130x874	GL215x456	GL215x988	GL265x1102
*Distance to Up(-)	0.15	0.25	0.58	1

* Distance to Up is computed as the Euclidean distance to the Utopia point in the normalized objective space.

Although these components require precise manufacturing processes and contribute to an increased embodied carbon footprint, their integration using the same material and consistent mass with the primary beam elements results in minimal variation in overall environmental impact.

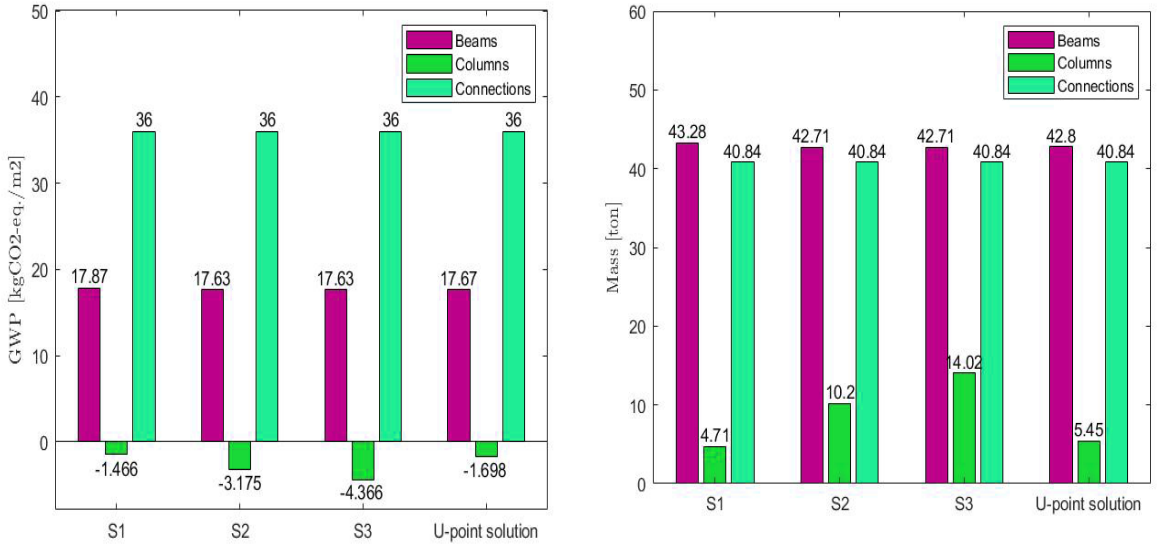

(a) GWP contribution per members (b) Mass contribution per member

Fig. 10. Contribution of member clusters for optimal solutions $S_{1,2,3}$ and the U-point solution in Case Study 2.1.

The penalty function values presented in **Table 13** confirm the feasibility of the optimized design solutions with respect to strength and serviceability requirements. In particular, the values of $\phi 1$ and $\phi 3$ are equal to 1 for all selected solutions, indicating that no strength or deflection constraint violations occur. The constant value of $\phi 2$ reflects the unchanged number of nodes/connections across the selected configurations, rather than a structural constraint violation. Therefore, the selected Pareto-optimal solutions differ mainly in terms of mass and environmental impact, while maintaining the same topological arrangement and satisfying the imposed feasibility constraints.

Table 13. Penalty function results for Case Study 2.1.

Penalty	Up	S1	S2	S3
φ1	1	1	1	1
φ2	50.6	50.6	50.6	50.6
φ3	1	1	1	1

Case Study 2.2 differs from 2.1 by expanding the design space to include a wider range of CS alternatives for diagonal elements, specifically using timber options. This modification stems from a comprehensive analysis of potential mass and GWP reduction benefits achievable through material diversification. **Fig. 11** illustrates the Pareto-optimal front, encompassing the full range of optimized design solutions. The front exhibits a distinct near-parabolic trend, followed by a linear segment characterized by greater population concentration. For in-depth analysis, three representative solutions — the two extreme points and an intermediate solution — are selected from the Pareto front.

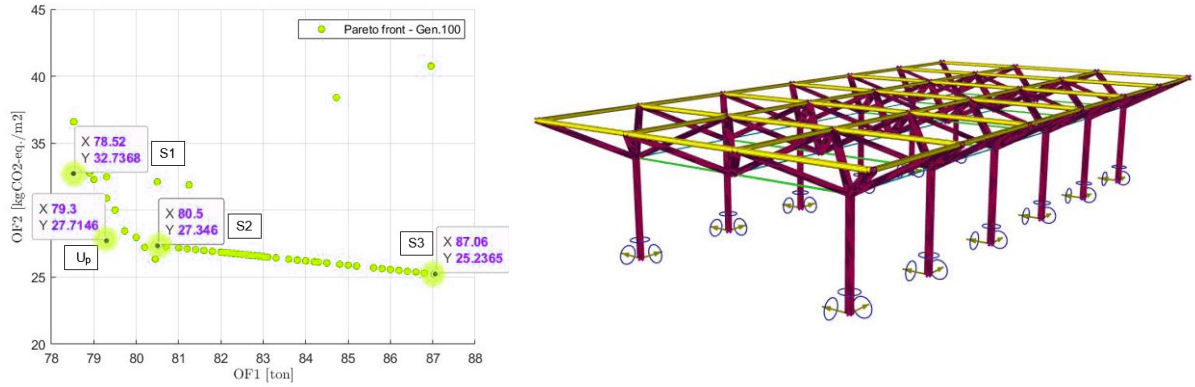

(a) Pareto optimal front (b) Optimal configuration

Fig. 11. Post-optimization Case Study 2.2

The corresponding optimized design variables and OF values are presented in **Table 14**. The penalty function values for the selected solutions are consistent with those observed in Case Study 2.1 (**Table 13**). Specifically, the penalties $\phi_{1,3}$ register a value of 1, indicating that the maximum allowable deflection is met and that all structural elements are feasible. This confirms the successful enforcement of these constraints during the optimization process. Concurrently, ϕ_2 remains constant across all solutions and is contingent upon the number of nodes in the arrangement.

Table 14. Case Study 2.2: Optimal design variable evaluation.

Params	Up	S1	S2	S3
OF1 (Mass)	79.3	79.3	80.51	87.06
OF2 (GWP)	27.71	32.74	27.35	25.24
Height (H) [m]	3	3	3	3
Divisions (x-dir.)	6	6	6	6
Divisions (y-dir.)	3	3	3	3
Long. Up.	CHS 355.6x6.3	CHS 355.6x6.3	CHS 355.6x6.3	CHS 355.6x6.3
Long. Low.	CHS 114.3x2.5	CHS 114.3x2.5	CHS 114.3x2.5	CHS 88.9x3
Transv. Up.	CHS 406.4x6	CHS 406.4x6	CHS 406.4x6	CHS 406.4x6
Transv. Low.	CHS 139.7x4	CHS 139.7x4	CHS 139.7x4	CHS 114.3x5
Diagonals	GL365x570	GL365x418	GL365x570	GL365x570
Columns	GL215x608	GL215x532	GL315x494	GL215x1368
*Distance to Up(-)	0.33	1.00	0.18	0.87

* Distance to Up is computed as the Euclidean distance to the Utopia point in the normalized objective space

A key finding of the optimal design variable analysis is the consistent selection of mixed-material configurations, featuring timber diagonals. This preference can be attributed to the significantly lower density of timber compared to steel, which directly contributes to the development of lightweight structural solutions. In these configurations, steel components exhibit a relatively uniform design. This

uniformity suggests that the optimizer effectively identifies elements operating at their maximum capacity, effectively meeting the structural specifications. However, slight variations in the cross-sectional dimensions of diagonals and columns are observed. These adjustments reflect the optimizer's attempt to balance the competing objectives of minimizing mass and environmental impact. Consequently, the increased use of timber leads to a significant reduction in the environmental objective function (OF2).

Regarding the shape variable, closed steel sections are preferred for each chord cluster, while rectangular glulam sections are used for the diagonals. The incorporation of glulam diagonals results in a 20% reduction in structural mass compared to Case study 2.1. Moreover, the environmental impact (GWP) is substantially reduced, yielding a 45% decrease in CO_2 emissions. All optimized designs maintain a 6x3 modular division layout, ensuring a consistent number of connections and associated GWP. The production stage remains a significant contributor to the overall carbon impact, primarily due to the contributions of the connection nodes (**Fig. 12**).

Distinct trends are observed in the beam component contributions, significantly influenced by the optimizer's selection of timber diagonals. In the first scenario, beams predominantly exhibited positive GWP values; however, the introduction of timber diagonals effectively reduces the embodied energy of these structural elements. Notably, although larger sections are allocated to columns, the GWP reduction achieved through the timber diagonals surpasses that of the columns. This is primarily attributed to the numerical dominance of diagonal elements, which outnumber the vertical columns by a factor of six. Negative GWP values associated with timber components are attributed to biogenic carbon storage and end-of-life credits (Module D), in accordance with EN 15804.

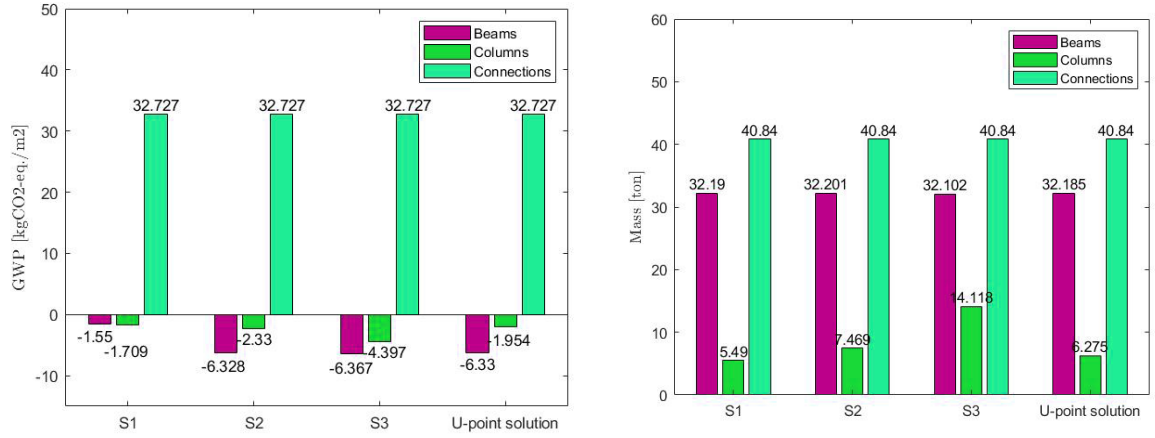

(a) GWP contribution per member (b) Mass contribution per member

Fig. 12. Contribution of member clusters for optimal solutions $S_{1,2,3}$ and the U-point solution in Case Study 2.2.

All optimization analyses were performed on a workstation equipped with a 13th-generation Intel Core i9-13980HX processor and 32 GB of RAM. The computational time was mainly influenced by the complexity of the case study and the number of design variables involved. In particular, complete optimization runs for Case Study 1 typically required on the order of a few hours (approximately 2–3 hours), whereas the increased model complexity and additional design variables in Case Study 2, 2.1 and 2.2 resulted in longer computational times, ranging from several hours up to overnight runs. These computational efforts were considered acceptable within the context of preliminary design exploration.

4 Conclusions

This study demonstrates the efficacy of incorporating Life Cycle Assessment (LCA) within a Structural Optimization (SO) framework for the sustainable design of steel and hybrid framed structures. The integrated framework, built upon parametric modeling within GH, proved to be an accessible and efficient tool for preliminary design evaluations. Its visual programming language (VPL) interface allows rapid exploration of design alternatives and seamless integration of structural analysis with Life Cycle Assessment (LCA). This approach significantly streamlined the design process, enabling efficient assessment of complex structural behaviors and environmental impacts.

The framework's applicability and adaptability across different material types were validated through case studies of steel and hybrid steel-timber space-frame structures. Case Study 1 explored a steel-only space-frame, focusing on optimizing cross-sections and member counts. Case Study 2 expanded this to hybrid steel-timber frames, with Subcase 2.1 focusing on minimizing mass with steel and moderate GWP reduction, and Subcase 2.2 balancing mass and GWP reduction through strategic timber integration. The successful optimization of these structures, incorporating Eurocode 3 and 5 constraints, demonstrated the framework's robustness. The consistent penalty function results, coupled with the optimizer's ability to select mixed-material configurations, particularly evident in Case Study 2.2, highlighted its adaptability to diverse material properties and design requirements. Moreover, the study effectively investigated the viability of design solutions that concurrently minimize total embodied energy and material consumption, encompassing optimization of size, shape, and topology. The multi-objective optimization (MOO) approach, utilizing both structural and environmental objective functions, revealed critical trade-offs and facilitated the identification of optimal compromise solutions. Notably, the 20% mass reduction and 45% GWP reduction achieved in Case Study 2.2 demonstrated the potential for significant improvements through integrated design strategies. The cradle-to-grave LCA approach, coupled with cross-sectional optimization and strategic material selection, further underscored the effectiveness of minimizing both material consumption and embodied energy.

This research successfully delivered a practical and adaptable framework for sustainable structural design. The integration of parametric modeling with LCA and MOO techniques provides a powerful tool for early-stage design decisions, enabling the development of resource-efficient and environmentally responsible structures. LCA incorporation in structural design is consistent with global trends for sustainable construction policies. The developed methodology allows proactive compliance with governmental and organizational regulations regarding carbon emissions and resource efficiency. Findings are directly applicable in industries related to high-performance structures (e.g., industrial buildings, stadiums), and projects pursuing environmental certifications (such as LEED, BREEAM). The methodology enables informed decision-making across a wide range of construction scenarios. This integration is expected to transform the approach to LCA inclusion in SO by enabling the simultaneous achievement of performance and environmental objectives.

A critical challenge identified in this work is the absence of native GWP data libraries within GH. This necessitates the development of a complete user-generated inventory for all material components, a process that requires significant additional effort and introduces the potential for data inconsistencies. However, the automation of this inventory generation and integration process would significantly enhance design workflow efficiency and data reliability. While this challenge persists, the results demonstrate the feasibility and added value of integrated approaches towards resource-efficient and environmentally responsible construction.

Funding Statement

Dr. Laura Sardone carried out this study within the RETURN Extended Partnership and received funding from the European Union Next-GenerationEU (National Recovery and Resilience Plan – NRRP, Mission 4, Component 2, Investment 1.3 – D.D. 1243 2/8/2022, PE0000005).

Dr. Giulia Angelucci gratefully acknowledges the financial support of the Research Project No. CN1221844D08208F from Sapienza University of Rome under the umbrella of the national program PNRR – CN1 – Spoke 5 (Directorial Decree no. 1031 of June, 17th, 2022).

Funding from the above research projects is greatly appreciated. The opinions and conclusions presented by the authors do not necessarily reflect those of the funding agencies.

CRediT authorship contribution statement

Laura Sardone: Conceptualization, Methodology, Software, Validation, Formal Analysis, Investigation, Resources, Data Curation, Writing - Original Draft, Visualization, Supervision, Project administration, Funding acquisition. **Giulia Angelucci:** Validation, Writing - Review and Editing, Visualization, Project administration, Funding acquisition.

Conflict of Interest

All authors certify that they have no affiliations with or involvement in any organization or entity with any financial interest or non-financial interest in the subject matter or materials discussed in this manuscript.

Data availability statement

The data will be made openly accessible in a GitHub repository upon request.

References

[1] IEA. Key world energy statistics. International Energy Agency, 2021.
[2] Hasegawa T. Environmentally sustainable buildings: challenges and policies. OECD Publishing, 2003.
[3] European Parliament. Directive 2010/31/EU of the European Parliament and of the Council of 19 May 2010 on the energy performance of buildings (recast). Official Journal of the European Union 2010; 153: 13–35.
[4] European Commission. The European Green Deal. Communication, 2019. Brussels, Belgium.
[5] Crawford RH. Greenhouse Gas Emissions of Global Construction Industries. IOP Conference Series: Materials Science and Engineering 2022; 1218(1): 012047. https://doi.org/10.1088/1757-899x/1218/1/012047.
[6] ISO 14044:2006. Environmental management - Life cycle assessment – Requirements and guidelines. First edition 2006. https://standards.iteh.ai/catalog/standards/sist/b3d74118-4c9f-4f3e-b556- 11d704441abb/iso-14044-2006.
[7] ISO 14040:2006. Environmental management — Life cycle assessment — Principles and framework 2006; 235–248. https://www.iso.org/obp/ui/#iso:std:iso:14040:ed-2:v1:en.
[8] Yeo D, Gabbai RD. Sustainable design of reinforced concrete structures through embodied energy optimization. Energy and buildings 2011; 43(8): 2028-2033. http://dx.doi.org/10.1016/j.enbuild.2011.04.014.
[9] Kaveh A, Mahdavi VR. Colliding bodies optimization: a novel meta-heuristic method. Computers & Structures 2014; 139: 18-27. http://dx.doi.org/10.1016/j.compstruc.2014.04.005.
[10] Laguardia R, Franchin P, Tesfamariam S. Risk-based optimization of concentrically braced tall timber buildings: Derivative free optimization algorithm. Earthquake Engineering & Structural Dynamics 2024; 53(1): 179-199. http://dx.doi.org/10.1002/eqe.4015.
[11] Bendsøe MP. Optimal shape design as a material distribution problem. Structural optimization 1989; 1: 193-202. http://dx.doi.org/10.1007/BF01650949.
[12] Angelucci G, Quaranta G, Mollaioli F. Topology optimization of multi-story buildings under fully non-stationary stochastic seismic ground motion. Structural and Multidisciplinary Optimization 2022; 65(8): 217. http://dx.doi.org/10.1007/s00158-022-03319-5.
[13] Angelucci G, Spence SM, Mollaioli F. An integrated topology optimization framework for three-dimensional domains using shell elements. The Structural Design of Tall and Special Buildings 2021; 30(1): e1817. http://dx.doi.org/10.1002/tal.1817.
[14] Haslinger J, Mäkinen RAE. A Mathematical Introduction to sizing and shape optimization. In: Advances in Design and Control - Introduction to Shape Optimization: Theory, Approximation, and Computation, SIAM 2003; 13-95. ISBN:978-0-89871-536-1.
[15] Bremicker M, Papalambros PY, Chirehdast M, Kikuchi N. Integrated Topology and Shape Optimization in Structural Design. Mechanics of Structures and Machines 1991; 19(4): 551–587. https://doi.org/10.1080/08905459108905156.
[16] Meng X, Xiong Y, Xie YM, Sun Y, Zhao, ZL. Shape–thickness–topology coupled optimization of free-form shells. Automation in Construction 2022; 142: 104476. https://doi.org/10.1016/j.autcon.2022.104476
[17] Sardone L, Fiore A, Manuello A, Greco R. Performative Structural Design Optimization: Generative Algorithm for a Preliminary Study of a Voided Beam. Applied Sciences 2022; 12(17): 8663. https://doi.org/10.3390/app12178663.
[18] Frangedaki E, Sardone L, Lagaros ND. Design Optimization of Tree-Shaped Structural Systems and Sustainable Architecture Using Bamboo and Earthen Materials. Journal of Architectural Engineering 2021; 27(4). https://doi.org/10.1061/(ASCE)AE.1943-5568.0000492.
[19] Russo D, Rizzi C. Structural optimization strategies to design green products. Computers in Industry 2014; 65(3): 470–479. https://doi.org/10.1016/j.compind.2013.12.009
[20] Mayyas AT, Qattawi A, Mayyas AR, Omar MA. Life cycle assessment-based selection for a sustainable lightweight body-in-white design. Energy 2012; 39(1): 412–425. https://doi.org/10.1016/j.energy. 2011.12.033.
[21] Morsi DMA, Othman AAE, Ehab A, Ismaeel WSE. BIM-based life cycle assessment for different structural

system scenarios of a residential building. Ain Shams Engineering Journal 2022; 13(6): 101802. https://doi.org/10.1016/j.asej.2022.101802.
[22] Russo D, Serafini M. Anticipating the Identification of Contradictions in Eco-design Problems. Procedia Engineering 2015; 131: 1011-1020. https://doi.org/10.1016/j.proeng.2015.12.419.
[23] Jacquemin L, Pontalier PY, Sablayrolles C. Life cycle assessment (LCA) applied to the process industry: a review. The International Journal of Life Cycle Assessment 2012; 17(8): 1028–1041. https://doi.org/10.1007/s11367-012-0432-9.
[24] Tao J, Chen Z, Yu S, Liu Z. Integration of Life Cycle Assessment with computer-aided product development by a feature-based approach. Journal of Cleaner Production 2016; 143: 1144–1164. https://doi.org/10.1016/j.jclepro.2016.12.005.
[25] Drewniok MP, Campbell J, Orr J. The Lightest Beam Method – A methodology to find ultimate steel savings and reduce embodied carbon in steel framed buildings. Structures 2020; 27: 687-701. https://doi.org/10.1016/j.istruc.2020.06.015.
[26] Wang W, Zmeureanu R, Rivard H. Applying multi-objective genetic algorithms in green building design optimization. Building and environment 2005; 40(11): 1512–1525. https://doi.org/10.1016/j.buildenv.2004.11.017.
[27] Schwartz Y, Raslan R, Mumovic D. Implementing multi objective genetic algorithm for life cycle carbon footprint and life cycle cost minimisation: A building refurbishment case study. Energy 2016; 97: 58–68. http://dx.doi.org/10.1016/j.energy.2015.11.056.
[28] Balasbaneh AT, Ramli MZ. A comparative life cycle assessment (LCA) of concrete and steel-prefabricated prefinished volumetric construction structures in Malaysia. Environmental Science and Pollution Research 2020; 27(34): 43186–43201. https://doi.org/10.1007/s11356-020-10141-3.
[29] Xu X, You J, Wang Y, Luo Y. Analysis and assessment of life-cycle carbon emissions of space frame structures. Journal of Cleaner Production 2023; 385: 135521. http://dx.doi.org/10.1016/j.jclepro.2022.135521
[30] Mimendi L, Lorenzo R, Li H. An innovative digital workflow to design, build and manage bamboo structures. Sustainable Structures 2022; 2(1).
[31] EN 15978:2011. Sustainability of Construction Works - Assessment of Environmental Performance of Buildings - Calculation Method, 2011.
[32] EN 15804:2012+A2:2019. Sustainability of construction works - Environmental product declarations - Core rules for the product category of construction products, 2022.
[33] Preisinger C, Heimrath M. Karamba - A Toolkit for Parametric Structural Design. Structural Engineering International 2014; 24(2): 217–221. https://doi.org/10.2749/101686614x13830790993483.
[34] EN 1993-1-1: Eurocode 3: Design of steel structures - Part 1-1: General rules and rules for buildings. [Authority: The European Union Per Regulation 305/2011, Directive 98/34/EC, Directive 2004/18/EC].
[35] EN 1995-1-1:2004+A1. Eurocode 5: Design of timber structures - Part 1-1: General - Common rules and rules for buildings. 2008.
[36] NTC 2018 Azioni sulle costruzioni – Supplemento ordinario n. 8 alla GAZZETTA UFFICIALE Chap.3 - 3.3:52-56.
[37] Gu C, Gu H, Gong M, Blackadar J, Zahabi N. Comparison of using two LCA software programs to assess the environmental impacts of two institutional buildings. Sustainable Structures 2024; 4(1):1-13. http://dx.doi.org/10.54113/j.sust.2024.000034.
[38] Zitzler E, Laumanns M, Thiele L. SPEA2: Improving the strength pareto evolutionary algorithm. Report in ETH Library 2001. https://doi.org/10.3929/ethz-a-004284029.
[39] Octopus; Food4Rhino. Available at: https://www.food4rhino.com/en/app/octopus (accessed January 2025).
[40] IronPython - the Python programming language for .NET. Available at: https://ironpython.net/documentation/dotnet/ (accessed January 2025).
[41] Lan, TT. Space frame structures. In: Structural engineering handbook 1999; 13(4).
[42] BS EN 1991-1-4:2005+A1:2010 - Wind actions 2005; ISBN 978 0 580 68497 5.
[43] Harte AM. Mass timber–the emergence of a modern construction material. Journal of Structural Integrity and Maintenance 2017; 2(3): 121-132. http://dx.doi.org/10.1080/24705314.2017.1354156
[44] Angelucci G, Mollaioli F, Molle M, Paris S. Performance assessment of timber high-rise buildings: Structural and technological considerations. The Open Construction & Building Technology Journal 2022; 16(1): 1-12. http://dx.doi.org/10.2174/18748368-v16-e2206270.
[45] Lu L, Anderson-Cook CM, Robinson TJ. Optimization of Designed Experiments Based on Multiple Criteria Utilizing a Pareto Frontier. Technometrics 2011; 53(4): 353–365. https://doi.org/10.1198/TECH.2011.10087.